International Journal of Modern Physics B
Vol. 31 (2017) 1750137 (23 pages)

DOI: 10.1142/S0217979217501375

Finite-difference method applied for eight-band kp model for $Hg_{1-x}Cd_xTe/HgTe$ quantum well

Michał Marchewka

Faculty of Mathematics and Natural Sciences,
Centre for Microelectronics and Nanotechnology,
University of Rzeszów,
Pigonia 1, 35-959 Rzeszów, Poland
marmi@ur.edu.pl

Received 6 October 2016
Revised 20 January 2017
Accepted 16 February 2017
Published 20 April 2017

In this work the finite-difference method (FDM) is presented for the undoped $Hg_{1-x}Cd_xTe/HgTe$ quantum well (QW) which allows to calculate the band structures based on Kane's 8×8 **kp** model including all second-order terms representing the remote-band contributions. In particular the common central-difference form is employed in the discretization procedure. The FDM is applied in the envelope function approach (EFA) for the [001]-oriented system for two cases: without a magnetic field ($B = 0$) and with a magnetic field perpendicular to the layer ($B\|z$). A proposed presented method can solve all the states simultaneously and can be used for a wide range of temperatures and widths of QW for different values of x for $Hg_{1-x}Cd_xTe/HgTe$ QW as well as for more complex structures, e.g., asymmetric QW, double quantum wells (DQWs), multiple quantum wells (MQWs) and for the so-called 3D topological insulator with a strained HgTe layer. The results obtained by this method are in a complete agreement with the previous ones. Based on that it is shown that the different x–Cd compounds in the barrier as well as in the QW make the critical width different than 6.4 nm for HgTe QW. What is also very interesting from the application point of view of the strained mixed HgCdTe QW is that for a different width and a different mismatch lattice it is possible to observe the influence of the upper and lower parts of the Dirac cone in, e.g., a magneto-transport experiment.

Keywords: Finite-difference method; Dirac point; 8×8 **kp**.

PACS numbers: 74.20.Pq, 73.61.Ga, 73.20.-r

1. Introduction

The $Hg_{1-x}Cd_xTe/HgTe$ quantum wells (QWs) are heterostructures of type III (Ref. 1) which depending on the width of QW have normal or inverted subband structures.[2] For such materials the 8×8 **kp** model[3] (including spin splitting) allows to, with successes, interpret a lot of experimental data,[4–13] and is also used by other authors.[2,14–17]

Because the Schrödinger equation with energy-dependent effective mass with nonlinear eigenvalue problem cannot be solved directly, a few numerical methods [transfer matrix method,[18–20] the shooting method,[21] finite-element method (FEM),[22] the plane-wave expansion method[23–25] or finite-difference method (FDM)[26–29]] have been proposed to solve the nonparabolic Schrödinger equation.

This paper shows the FDM applied for an 8×8 **kp** model[11] to solve numerically the differential Schrödinger equation. In particular the common central-difference form is employed in the discretization procedure. In this case we consider an eight-band description of the band structure including all second-order terms representing the remote-band contributions with $\boldsymbol{J} = \pm 3/2$, heavy hole and light hole bands and $\boldsymbol{J} = \pm 1/2$ along with the $\boldsymbol{J} = \pm 1/2$ conduction band states and $\boldsymbol{J} = \pm 1/2$ spin–orbit split-off states. The calculation of energy spectrum is provided in the framework of the envelope function approach (EFA) for the [001]-oriented system where z-axis coincides with the growth direction of the quantum well.

The papers is organized as follows: in Sec. 2 the 8×8 **kp** band model is presented for two cases: without magnetic field and with magnetic field perpendicular to the layer ($B \| z$). In Sec. 3 the formulae for FDM will be developed for a central-difference form. The results of the calculation for the typical QW structures based on $Hg_{1-x}Cd_xTe/HgTe$ for different widths of QW are reported in Sec. 4. The electronic band structures ($B = 0$) and the electronic Landau levels (LLs) ($B \neq 0$) calculated by the presented method remain in full compatibility with previous reports at the same time confirming the effectiveness of the presented method. Some conclusions are presented in Sec. 5. The matrices which are needed to solve the 8×8 **kp** band model in the presented method for the barriers and for QW as well as for all interfaces for $B = 0$ are presented in Appendix A.

2. The 8×8 kp Model

The Schrödinger equation for 8×8 Hamiltonian for the two-dimensional vector of envelope functions can be simply written as

$$H\Psi(r) = E\Psi(r), \tag{1}$$

where for such a system the carrier wavefunction can be written as

$$\Psi(r) = \sum_n F_n(r) u_n(r). \tag{2}$$

The $F_n(r)$ are the envelope functions and the sum index n varies from 1 to 8. The $u_n(r)$ are Bloch functions which are the same in the barrier and the well layers. F_n can be represented as

$$F_n = \exp[i(k_x x + k_y y)] f_n(z), \tag{3}$$

where k_x and k_y are the wave vector components in the plane of QW.

Energy levels and envelope function coefficients can be found from the simultaneous solution of the system of coupled differential equations.[11] The Hamiltonian in such system takes the following form[11]:

$$H_0 = \begin{bmatrix}
T & 0 & \frac{-1}{\sqrt{2}}Pk_+ & \sqrt{\frac{2}{3}}Pk_z & \frac{1}{\sqrt{6}}Pk_- & 0 & \frac{-1}{\sqrt{3}}Pk_z & -\frac{1}{\sqrt{3}}Pk_- \\
0 & T & 0 & -\frac{1}{\sqrt{6}}Pk_+ & \sqrt{\frac{2}{3}}Pk_z & \frac{1}{\sqrt{2}}Pk_- & -\frac{1}{\sqrt{3}}Pk_+ & \frac{1}{\sqrt{3}}Pk_z \\
-\frac{1}{\sqrt{2}}k_-P & 0 & U+V & -\bar{S}_- & R & 0 & \frac{1}{\sqrt{2}}\bar{S}_- & -\sqrt{2}R \\
\sqrt{\frac{2}{3}}k_zP & -\frac{1}{\sqrt{6}}k_-P & -\bar{S}_-^\dagger & U-V & C & R & \sqrt{2}V & -\sqrt{\frac{3}{2}}\tilde{S}_- \\
\frac{1}{\sqrt{6}}k_+P & \sqrt{\frac{2}{3}}k_zP & R^\dagger & C^\dagger & U-V & \bar{S}_+^\dagger & -\sqrt{\frac{3}{2}}\tilde{S}_+ & -\sqrt{2}V \\
0 & \frac{1}{\sqrt{2}}k_+P & 0 & R^\dagger & \bar{S}_+ & U+V & \sqrt{2}R^\dagger & \frac{1}{\sqrt{2}}\bar{S}_+ \\
-\frac{1}{\sqrt{3}}k_zP & -\frac{1}{\sqrt{3}}k_-P & \frac{1}{\sqrt{2}}\bar{S}_-^\dagger & \sqrt{2}V & -\sqrt{\frac{3}{2}}\tilde{S}_+^\dagger & \sqrt{2}R & U-\Delta & C \\
-\frac{1}{\sqrt{3}}k_+P & \frac{1}{\sqrt{3}}k_zP & -\sqrt{2}R^\dagger & -\sqrt{\frac{3}{2}}\tilde{S}_-^\dagger & -\sqrt{2}V & \frac{1}{\sqrt{2}}\bar{S}_+^\dagger & C^\dagger & U-\Delta
\end{bmatrix} \tag{4}$$

where

$$k_{||}^2 = k_x^2 + k_y^2, \quad k_\pm = k_x \pm ik_y, \quad k_z = -i\partial/\partial z,$$

$$T = E_c(z) + \frac{\hbar^2}{2m_0}[(2F+1)k_{||}^2 + k_z(2F+1)k_z],$$

$$U = E_v(z) - \frac{\hbar^2}{2m_0}(\gamma_1 k_{||}^2 + k_z\gamma_1 k_z),$$

$$V = -\frac{\hbar^2}{2m_0}(\gamma_2 k_{||}^2 - 2k_z\gamma_2 k_z),$$

$$R = -\frac{\hbar^2}{2m_0}\sqrt{3}(\mu k_+^2 - \bar{\gamma}k_-^2),$$

$$\bar{S}_{\pm} = -\frac{\hbar^2}{2m_0}\sqrt{3}k_{\pm}(\{\gamma_3, k_z\} + [\kappa, k_z]),$$

$$\tilde{S}_{\pm} = -\frac{\hbar^2}{2m_0}\sqrt{3}k_{\pm}\left(\{\gamma_3, k_z\} - \frac{1}{3}[\kappa, k_z]\right), \tag{5}$$

$$C = \frac{\hbar^2}{m_0}k_{-}[\kappa, k_z].$$

$[A, B] = AB - BA$ is the usual commutator and $\{A, B\} = AB + BA$ is the anti-commutator for the operators A and B; P is the Kane momentum matrix element; $E_c(z)$ and $E_v(z)$ are the conduction and valence band edges, respectively; Δ is the spin–orbit splitting energy; and γ_1, γ_2, γ_3, κ and F describe the coupling to the remote bands. The μ and $\bar{\gamma}$ are parameters according to $\mu = (\gamma_3 - \gamma_2)/2$ and $\bar{\gamma} = (\gamma_3 + \gamma_2)/2$. The band structure parameters for HgTe and CdTe used in calculations are listed in Table 1. The dependence of the bandgap for $Hg_{1-x}Cd_xTe$ as a function of the temperature and composition x is determined from the empirical expression according to Becker *et al.*[30]

Table 1. Band structure parameters of HgTe and CdTe.

	E_g (eV)	E_v (meV)	Δ (eV)	$E_p = 2m_0P^2/\hbar^2$ (eV)	F	γ_1	γ_2	γ_3	κ
HgTe	−0.303	0	1.08	18.8	0	4.1	0.5	1.3	−0.4
CdTe	1.606	−570	0.91	18.8	−0.09	1.47	−0.28	0.03	−1.31

The valence band offset between HgTe and CdTe is taken to be equal to 570 ± 26 meV at $T = 5$ K.[30] Here 570 meV is used in the calculation. The FDM is developed for Hamiltonian H_0 [Eq. (4)] which is defined for [001]. The elements of strain tensor for $Hg_{1-x}Cd_xTe$/HgTe QW (which can be represented by Bir and Pikus Hamiltonian[11]) is neglected here. For the case of different QW orientations or for the strained 3D HgTe topological insulator (TI), the strain tensor plays a critical role and cannot be omitted (see Sec. 5).

2.1. *For $B \neq 0$*

For the magnetic field perpendicular to the layer ($B \| z$), following Ref. 31 the Hamiltonian H_0 looks as follows:

$$k \to k' = -i\nabla + \frac{e}{\hbar}\mathbb{A}, \tag{6}$$

where $\mathbb{A}$ is the magnetic vector potential: $\mathbf{B} = \nabla \times \mathbb{A}$. One possible Landau gauge for $\mathbf{B} = (0, 0, B)$ is $\mathbb{A} = (0, Bx, 0)$. The wave vector components k_x and k_y are nowexpressed in terms of harmonic oscillator creation, $a^{\dagger}$, and annihilation,

a, operators:

$$a = \left(\frac{\hbar}{2eB}\right)^{1/2}(k_x - ik_y), \tag{7}$$

$$a^\dagger = \left(\frac{\hbar}{2eB}\right)^{1/2}(k_x + ik_y). \tag{8}$$

As for the case $B = 0$, the component k_z which is along the direction of the applied magnetic field is replaced by $-i\partial/\partial z$. The operators a and $a^\dagger$ have the following properties:

$$[a, a^\dagger] = 1, \quad a^\dagger a\phi_n = n\phi_n, \quad a\phi_n = \sqrt{n}\phi_{n-1}, \quad a^\dagger\phi_n = \sqrt{n+1}\phi_{n+1}, \tag{9}$$

where $n = 0, 1, 2, \ldots$ are the eigenvalues of the operator $a^\dagger a$ and ϕ_n are the harmonic oscillators wavefunction. Applying relations from Eqs. (7) and (8) into $k_{||}$ and $k_\pm$ we have $k_{||}^2 = s(2a^\dagger a + 1)$, $k_\pm \equiv k_{+/-} = \sqrt{2s}(a^{\dagger/1})$ (where $\pm \equiv +/- = \dagger/1$, $s = eB/\hbar$), and then we get the shape of the matrix elements T, U, V, R, $\bar{S}_\pm$, $\tilde{S}_\pm$ and C inside the Hamiltonian H_0:

$$\begin{aligned}
T &= E_c(z) + \frac{\hbar^2}{2m_0}[s(2F+1)(2a^\dagger a + 1) + k_z(2F+1)k_z],\\
U &= E_v(z) - \frac{\hbar^2}{2m_0}(s\gamma_1(2a^\dagger a + 1) + k_z\gamma_1 k_z),\\
V &= -\frac{\hbar^2}{2m_0}(s\gamma_2(2a^\dagger a + 1) - 2k_z\gamma_2 k_z),\\
R &= -\frac{\hbar^2}{2m_0}2\sqrt{3}s(\mu a^\dagger a^\dagger - \bar{\gamma}aa),\\
\bar{S}_\pm &= -\frac{\hbar^2}{2m_0}\sqrt{6}\sqrt{s}(a^{\dagger/1})(\{\gamma_3, k_z\} + [\kappa, k_z]),\\
\tilde{S}_\pm &= -\frac{\hbar^2}{2m_0}\sqrt{6}\sqrt{s}(a^{\dagger/1})\left(\{\gamma_3, k_z\} - \frac{1}{3}[\kappa, k_z]\right),\\
C &= \frac{\hbar^2}{m_0}\sqrt{2s}a[\kappa, k_z].
\end{aligned} \tag{10}$$

Using these relations we get the Hamiltonian in Eq. (4) as a function of a, $a^\dagger$ and $-i\partial/\partial z$, and as before the band structures parameters and their z dependence.

The total wavefunction for such a system can be written as[3]

$$\Psi_N(\mathbf{r}) = \exp\left(-i\frac{X}{l_c^2}y\right)\begin{pmatrix} f_1^{(N)}(z)\phi_N \\ f_2^{(N)}(z)\phi_{N+1} \\ f_3^{(N)}(z)\phi_{N-1} \\ f_4^{(N)}(z)\phi_N \\ f_5^{(N)}(z)\phi_{N+1} \\ f_6^{(N)}(z)\phi_{N+2} \\ f_7^{(N)}(z)\phi_N \\ f_8^{(N)}(z)\phi_{N+1} \end{pmatrix}, \tag{11}$$

where $X = -l_c^2 k_y$ is the center-of-motion coordinate and restrictions on the new quantum numbers N. Furthermore we have to add, after Weiler,[32] the Zeeman term (H^Z) to the Hamiltonian H_0:

$$H^Z = \hbar\frac{eB}{m_0}\begin{pmatrix} \frac{1}{2} & 0 & 0 & 0 & 0 & 0 & 0 & 0 \\ 0 & -\frac{1}{2} & 0 & 0 & 0 & 0 & 0 & 0 \\ 0 & 0 & -\frac{3}{2}\kappa & 0 & 0 & 0 & 0 & 0 \\ 0 & 0 & 0 & -\frac{1}{2}\kappa & 0 & 0 & -\frac{\kappa+1}{\sqrt{2}} & 0 \\ 0 & 0 & 0 & 0 & \frac{1}{2}\kappa & 0 & 0 & -\frac{\kappa+1}{\sqrt{2}} \\ 0 & 0 & 0 & 0 & 0 & \frac{3}{2}\kappa & 0 & 0 \\ 0 & 0 & 0 & -\frac{\kappa+1}{\sqrt{2}} & 0 & 0 & -\left(\kappa+\frac{1}{2}\right) & 0 \\ 0 & 0 & 0 & 0 & -\frac{\kappa+1}{\sqrt{2}} & 0 & 0 & \left(\kappa+\frac{1}{2}\right) \end{pmatrix}. \tag{12}$$

After inserting the wavefunction [Eq. (11)] into the Hamiltonian [Eq. (1)] with the elements defined in Eq. (10) and making use of the properties of the operators a and $a^\dagger$ given in Eq. (9), we get the shape of the Hamiltonian H_0' for $B \neq 0$:

$$H_0' = E^q(z) + \hbar/2m_0 * H' + H^Z, \tag{13}$$

where H' is given by Eq. (14):

$$H' = \begin{bmatrix}
s(2F+1)(2n+1) & 0 & -P\sqrt{sn} & \sqrt{\frac{2}{3}}Pk_z & -\frac{2\sqrt{3}}{3}P\sqrt{s(n+1)} & 0 & -\frac{1}{\sqrt{3}}Pk_z & -\sqrt{\frac{2}{3}}P\sqrt{s(n+1)} \\
+k_z(2F+1)k_z & & & & & & & \\
0 & s(2F+1)(2n+3) & 0 & -\frac{2\sqrt{3}}{3}P\sqrt{s(n+1)} & \sqrt{\frac{2}{3}}Pk_z & P\sqrt{s(n+2)} & -\sqrt{\frac{2}{3}}P\sqrt{s(n+1)} & \frac{1}{\sqrt{3}}Pk_z \\
 & +k_z(2F+1)k_z & & & & & & \\
-P\sqrt{sn} & 0 & -s(2n-1)(\gamma_1+\gamma_2) & 2\sqrt{6sn}(\{\gamma_3,k_z\} & -2\sqrt{3}s(\mu\sqrt{(n+2)(n+3)} & 0 & 2\sqrt{3sn}(\{\gamma_3,k_z\} & 2\sqrt{6}s(\mu\sqrt{(n+2)(n+3)} \\
 & & $-k_2(r_1-2r_2)k_2$ & $+[k,k_z])$ & $-\bar{\gamma}\sqrt{n(n+1)})$ & & $-[\kappa,k_z])$ & $-\bar{\gamma}\sqrt{n(n+1)})$ \\
\sqrt{\frac{2}{3}}k_zP & -\frac{2\sqrt{3}}{3}P\sqrt{s(n+1)} & -2\sqrt{6sn} & -s(2n+1)(\gamma_1-\gamma_2) & 2\sqrt{2s(n+1)}[\kappa,k_z] & -2\sqrt{3}s(\mu\sqrt{(n+3)(n+4)} & -2\sqrt{2}(s\gamma_2(n+1) & -6\sqrt{s(n+1)} \\
 & & $\times(\{\gamma_3,k_z\}-[\kappa,k_z])^\dagger$ & $-k_z(\gamma_1+2\gamma_2)k_z$ & & $-\bar{\gamma}\sqrt{(n+1)(n+2)})$ & $-k_z\gamma_2k_z)$ & $\times(\{\gamma_3,k_z\}-\frac{1}{3}[\kappa,k_z])$ \\
\frac{2\sqrt{3}}{3}P\sqrt{s(n+1)} & \sqrt{\frac{2}{3}}k_zP & -2\sqrt{3}s(\mu\sqrt{(n-1)(n-2)} & $(2\sqrt{2sn}[\kappa,k_z])^\dagger$ & $-s(2n+3)(\gamma_1-\gamma_2)$ & $-(\sqrt{6s(n+2)}$ & $-6\sqrt{s(n+1)}$ & $2\sqrt{2}(s\gamma_2(n+2)$ \\
 & & $-\bar{\gamma}\sqrt{n(n+1)})^\dagger$ & & $-k_z(\gamma_1+2\gamma_2)k_z$ & $\times\{\gamma_3,k_z\}+[\kappa,k_z])^\dagger$ & $\times(\{\gamma_3,k_z\}-\frac{1}{3}[\kappa,k_z])$ & $-k_z\gamma_2k_z)$ \\
0 & $P\sqrt{s(n+2)}$ & 0 & $-2\sqrt{3}s(\mu\sqrt{n(n-1)}$ & $-2\sqrt{6s(n+2)}$ & $-s(2n+5)(\gamma_1+\gamma_2)$ & $-2\sqrt{6}s(\mu\sqrt{n(n-1)}$ & $-2\sqrt{3s(n+2)}$ \\
 & & & $-\bar{\gamma}\sqrt{(n+1)(n+2)})^\dagger$ & $\times(\{\gamma_3,k_z\}+[\kappa,k_z])$ & $-k_z(\gamma_1-2\gamma_2)k_z$ & $-\bar{\gamma}\sqrt{(n+1)(n+2)})^\dagger$ & $\times(\{\gamma_3,k_z\}+[\kappa,k_z])$ \\
-\frac{1}{\sqrt{3}}k_zP & -\sqrt{\frac{2}{3}}P\sqrt{s(n+1)} & $2(\sqrt{3sn}$ & $-2\sqrt{2}(s\gamma_2(n+1)$ & $(6\sqrt{s(n+1)}$ & $-2\sqrt{6}s(\mu\sqrt{(n+3)(n+4)}$ & $-s\gamma_1(2n+1)$ & $2\sqrt{2s(n+1)}$ \\
 & & $\times(\{\gamma_3,k_z\}+[\kappa,k_z]))^\dagger$ & $-k_z\gamma_2k_z)$ & $\times(\{\gamma_3,k_z\}-\frac{1}{3}[\kappa,k_z]))^\dagger$ & $-\bar{\gamma}\sqrt{(n+1)(n+2)})$ & $-k_z\gamma_1k_z$ & $\times[\kappa,k_z]$ \\
-\sqrt{\frac{2}{3}}P\sqrt{s(n+1)} & \frac{1}{\sqrt{3}}k_zP & $2\sqrt{6}s(\mu\sqrt{(n-1)(n-2)}$ & $(6\sqrt{s(n+1)}$ & $2\sqrt{2}(s\gamma_2(n+2)$ & $(-2\sqrt{3s(n+2)}$ & $(2\sqrt{2s(n+1)}$ & $-s\gamma_1(2n+3)$ \\
 & & $-\bar{\gamma}\sqrt{n(n+1)})^\dagger$ & $\times(\{\gamma_3,k_z\}-\frac{1}{3}[\kappa,k_z]))^\dagger$ & $-k_z\gamma_2k_z)$ & $\times(\{\gamma_3,k_z\}+[\kappa,k_z]))^\dagger$ & $\times([\kappa,k_z]))^\dagger$ & $-k_z\gamma_1k_z$
\end{bmatrix} \tag{14}$$

The FDM that is described in Sec. 3 can be applied here for Hamiltonian H' again as well as for H_0.

3. FDM for $B = 0$

The Hamiltonian, Eq. (4), is a quadratic polynomial in k_z, and the corresponding eigenfunction is F which is a function of z for fixed $k_{||}$ and E. The Schrödinger equation with the kinetic part of the Hamiltonian as a function of $k_{||}$ and $k_z = -i\partial/\partial z$ has a form

$$H_0(k_{\|}, -i\partial/\partial z)F(k_{\|}; z) = E(k_{\|})F(k_{\|}; z). \tag{15}$$

For each point z the eigenvalue problem is written as

$$H_0(k_{||}, -i\partial/\partial z) \begin{bmatrix} F_1(k_{||}; z) \\ F_2(k_{||}; z) \\ F_3(k_{||}; z) \\ F_4(k_{||}; z) \\ F_5(k_{||}; z) \\ F_6(k_{||}; z) \\ F_7(k_{||}; z) \\ F_8(k_{||}; z) \end{bmatrix} = E(k_{||}) \begin{bmatrix} F_1(k_{||}; z) \\ F_2(k_{||}; z) \\ F_3(k_{||}; z) \\ F_4(k_{||}; z) \\ F_5(k_{||}; z) \\ F_6(k_{||}; z) \\ F_7(k_{||}; z) \\ F_8(k_{||}; z) \end{bmatrix}. \tag{16}$$

The H_0 can be represented as a sum of three matrices containing the sequences: H_0^a, which are independent of the operator k_z; H_0^b, dependent on k_z; and H_0^c, elements dependent on $k_z A k_z$:

$$H_0(k_{||}, -i\partial/\partial z) = H_0^a - iH_0^b\partial/\partial z + i\partial/\partial z H_0^c i\partial/\partial z. \tag{17}$$

The $k_{||}$ can be omitted because this is a fixed value which does not change along the z-direction. The functions F can be indexed by z_n and j so $F(k_{||}; z) \equiv F_j(z_n)$. The derivatives calculated with a central difference for $F_j(z_n)$ can be given as

$$\frac{\partial}{\partial z}F_j(z_n) = \frac{F_j(z_{n+1}) - F_j(z_{n-1})}{2\Delta z_n}, \tag{18}$$

for $\Delta z_n \equiv z_{n+1} - z_n$.

In practice the Hamiltonian H_0 includes four different types of elements $H_{i,j}$ (following Ref. 33). Each of them depends on the position z_n. The elements of the matrix H_0 now can be defined as $H_{i,j}(z_n)$. For each point z_n the derivatives have a different shape. For the matrix H_0^a [Eq. (17)] with no derivative operator we have

$$H_0^a = H_{i,j}^a(z_n)F_j(z_n). \tag{19}$$

The matrix $H_{i,j}^a(z_n)$ includes the elements proportional to $k_{||}$ and proportional to the momentum matrix element P together with the elements containing $E_c(z)$, $E_v(z)$, Δ and the combinations thereof.

The second component, H_0^b, on the right-hand side in Eq. (17) is a matrix whose elements are proportional to k_z and for two cases: $H_{i,j}^b(z_n)\frac{\partial}{\partial z}F_j(z_n)$ and $\frac{\partial}{\partial z}H_{i,j}^b(z_n)F_j(z_n)$ it takes the forms

$$H_{i,j}^b(z_n)\frac{\partial}{\partial z}F_j(z_n) = H_{i,j}^b(z_n)\frac{F_j(z_{n+1}) - F_j(z_{n-1})}{2\Delta z_n}, \tag{20}$$

$$\frac{\partial}{\partial z}H_{i,j}^b(z_n)F_j(z_n) = \frac{H_{i,j}^b(z_{n+1})F_j(z_{n+1}) - H_{i,j}^b(z_{n-1})F_j(z_{n-1})}{2\Delta z_n}. \tag{21}$$

The last component in Eq. (17), H_0^c, now is defined as $H_{i,j}^c(z_n)$ and for the elements between the operators k_z it takes the form

$$\begin{aligned}
&\frac{\partial}{\partial z}H_{i,j}^c(z_n)\frac{\partial}{\partial z}F_j(z_n)\\
&\quad = F_j(z_{n-1})\left(\frac{H_{i,j}^c(z_{n-1}) + H_{i,j}^c(z_n)}{2\Delta z_n^2}\right)\\
&\qquad + F_j(z_n)\left(-\frac{H_{i,j}^c(z_{n-1}) + H_{i,j}^c(z_n)}{2\Delta z_n^2} - \frac{H_{i,j}^c(z_{n+1}) + H_{i,j}^c(z_n)}{2\Delta z_n^2}\right)\\
&\qquad + F_j(z_{n+1})\left(\frac{H_{i,j}^c(z_{n+1}) + H_{i,j}^c(z_n)}{2\Delta z_n^2}\right).
\end{aligned} \tag{22}$$

The Hermitian properties of the Hamiltonian can be obtained by using the following finite-difference formulas. Applying Eqs. (19)–(22) is known as using symmetrizing boundary conditions for abrupt (step-like) interfaces.[34] The presented method is corrected as it was confirmed in the simulations of Meney *et al.*,[35] for InGaAsSb/AlGaSb QW when the lowest conduction band is included in the Hamiltonian.

Starting from the left-hand side of the barrier (Fig. 1) by successive layers of the structure the finite-difference equations for each digitized point have to be defined for each point of the system.

The discretization of the eight equations [Eq. (16)] obtained for every grid point will produce a tridiagonal matrix of dimension $8N \times 8N$, where N is the number of grid points (see Fig. 1).

The $\mathbf{A}$ matrix is created from Eqs. (19) and (22) for each point. The matrices $\mathbf{B}$ and $\mathbf{C}$ are constructed with elements $H_{i,j}^{b,c}(z_{n-1}, z_{n+1})$ for $F_j(z_{n+1})$ and $F_j(z_{n-1})$ [Eqs. (20)–(22)].

The elements of each matrices $\mathbf{A}(z)$, $\mathbf{B}(z)$ and $\mathbf{C}(z)$ depend on the position z, and for z belonging to the quantum barrier (QB) or the QW the matrix $\mathbf{A}$ is written as

$$\mathbf{A}(z) = \frac{\hbar^2}{2m_0}\left[k_{||}^2\mathbf{A}_1(z) + \mathbf{A}_2(z) + \frac{2}{\Delta z^2}\mathbf{A}_3(z)\right] + \mathbf{E}^q(z), \tag{23}$$

where γ_1, γ_2, γ_3, κ and F are the parameters for the materials of the barriers (left or right) or the QW, respectively. The shape of each submatrix $\mathbf{A}_1(z)$, $\mathbf{A}_2(z)$, $\mathbf{A}_3(z)$ and $\mathbf{E}^q(z)$ is presented in Appendix A.

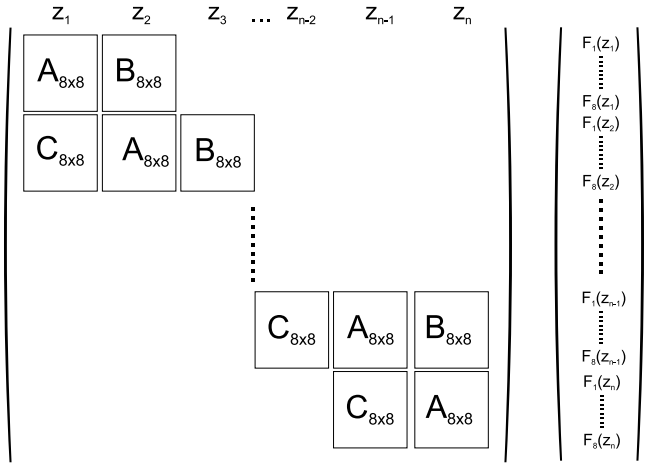

Fig. 1. The scheme of the $8N \times 8N$ matrix for eight-band **kp** model.

The $\mathbf{B}$ matrix is written as

$$\mathbf{B}(z) = \frac{\hbar^2}{2m_0}\left[\frac{-1}{\Delta z^2}\mathbf{A}_3(z) + \frac{-i}{2\Delta z}\mathbf{B}_1(z) + \left(\frac{-i}{2\Delta z}\right)^{\dagger}\mathbf{B}_2(z)\right]. \tag{24}$$

The shape of the $\mathbf{C}$ matrix is almost the same as $\mathbf{B}$ matrix. The coefficients between second and third submatrices in Eq. (24) are different. In case of $\mathbf{C}$ these coefficients are $\frac{i}{2\Delta z}$ and $(\frac{i}{2\Delta z})^{\dagger}$:

$$\mathbf{C}(z) = \frac{\hbar^2}{2m_0}\left[\frac{-1}{\Delta z^2}\mathbf{A}_3(z) + \frac{i}{2\Delta z}\mathbf{B}_1(z) + \left(\frac{i}{2\Delta z}\right)^{\dagger}\mathbf{B}_2(z)\right]. \tag{25}$$

Matrices $\mathbf{B}_1(z)$ and $\mathbf{B}_2(z)$ are also presented in Appendix A.

In case of boundaries between two materials it is necessary to define the matrices for two interfaces: at the boundary between QB and QW and at the boundary between QW and QB. Using Eqs. (19)–(22) we get for the first interface:

$$\mathbf{A}^{BW}(z_j) = \frac{\hbar^2}{2m_0}\left[k_{||}^2\mathbf{A}_1^B + \mathbf{A}_2^B + \mathbf{A}_3^B\frac{1}{\Delta z^2} + (\mathbf{A}_3^B + \mathbf{A}_3^W)\frac{1}{2\Delta z^2}\right] + \mathbf{E}^B, \tag{26}$$

where $\mathbf{A}^{BW}(z_j)$ is the last $\mathbf{A}(z_j)$ matrix at some z_j which is the last point of QB; $\mathbf{A}_i^{B/W}$ for $i = 1, 2, 3$ are the matrices $\mathbf{A}_i(z)$ defined for the barrier (B) or well (W) with the parameters for the barrier or well materials. $\mathbf{E}^B$ is a diagonal matrix with the elements $E_c(z)$, $E_v(z)$ and Δ (see Appendix A). If the matrix defined in Eq. (26) is the last one for QB then the matrix $\mathbf{B}^{BW}$ [after Eq. (22)] has a form

$$\mathbf{B}^{BW}(z_j) = \frac{\hbar^2}{2m_0}\left[-(\mathbf{A}_3^B + \mathbf{A}_3^W)\frac{1}{2\Delta z^2} + \mathbf{B}_1^{BW}\frac{i}{2\Delta z} + \mathbf{B}_2^{BW}\left(\frac{i}{2\Delta z}\right)^{\dagger}\right], \tag{27}$$

where the matrices $\mathbf{B}_1^{BW}$ and $\mathbf{B}_2^{BW}$ are similar to matrices $\mathbf{B}_1(z)$ and $\mathbf{B}_2(z)$, respectively (see Appendix A). The difference between them is as follows: the elements

of the matrices $\mathbf{B}_1(z)$ and $\mathbf{B}_2(z)$ which are proportional to γ_3 in the case of $\mathbf{B}_1^{BW}$ and $\mathbf{B}_2^{BW}$ are proportional to the term $(\gamma_3^B + \gamma_3^S + \kappa^B - \kappa^S)$, except for the matrix elements [4,8] and [5,7] of the matrix $\mathbf{B}_1^{BW}$ and [7,5] and [8,4] of the matrix $\mathbf{B}_2^{BW}$ which are proportional to the term $(\gamma_3^B + \gamma_3^S - \frac{1}{3}(\kappa^B - \kappa^S))$. Besides that both of the matrices at the interface have an additional term proportional to C element [see last line in Eq. (5)] that gives $\mathbf{B}_1^{BW}[4,5] = \mathbf{B}_1^{BW}[7,8] = \mathbf{B}_2^{BW}[5,4] = \mathbf{B}_2^{BW}[8,7] = 2k_-(\kappa^B - \kappa^S)$.

The $\mathbf{C}^{BW}(z_j)$ matrix at the z_j point is the same as in the case of the matrix defined for the area of the barrier with the parameters of the barrier material.

For the point z_{j+1} which is the first point of QW, the matrix $\mathbf{A}^{BW}(z_{j+1})$ is similar like that for $\mathbf{A}^{BW}(z_j)$ where instead the matrix describing the material of QB (with index B) is the matrix describing the material of QW (with index W):

$$\mathbf{A}^{BW}(z_{j+1}) = \frac{\hbar^2}{2m_0}\left[k_{||}^2\mathbf{A}_1^W + \mathbf{A}_2^W + \mathbf{A}_3^W\frac{1}{\Delta z^2} + (\mathbf{A}_3^B + \mathbf{A}_3^W)\frac{1}{2\Delta z^2}\right] + \mathbf{E}^W. \quad (28)$$

In this case the $\mathbf{B}^{BW}(z_{j+1})$ matrix is the same as in Eq. (24) for the area of QW, however $\mathbf{C}^{BW}(z_{j+1})$ matrix is written as

$$\mathbf{C}^{BW}(z_{j+1}) = \frac{\hbar^2}{2m_0}\left[-(\mathbf{A}_3^B + \mathbf{A}_3^W)\frac{1}{2\Delta z^2} + \mathbf{C}_1^{BW}\frac{-i}{2\Delta z} + \mathbf{C}_2^{BW}\left(\frac{-i}{2\Delta z}\right)^{\dagger}\right], \quad (29)$$

where the matrices $\mathbf{C}_1^{BW}$ and $\mathbf{C}_2^{BW}$ are similar to matrices $\mathbf{B}_1^{BW}$ and $\mathbf{B}_2^{BW}$, respectively (see above). The difference between them is as follows: the elements of the matrices $\mathbf{B}_1^{BW}$ and $\mathbf{B}_2^{BW}$ which are proportional to $(\gamma_3^B + \gamma_3^S + \kappa^B - \kappa^S)$ in the case of $\mathbf{C}_1^{BW}$ and $\mathbf{C}_2^{BW}$ are proportional to the term $(\gamma_3^B + \gamma_3^S + \kappa^S - \kappa^B)$. It is the same for the elements [4,8] and [5,7] of the matrix $\mathbf{C}_1^{BW}$ and [7,5] and [8,4] of the matrix $\mathbf{C}_2^{BW}$ which are proportional to the term $(\gamma_3^B + \gamma_3^S - \frac{1}{3}(\kappa^S - \kappa^B))$. The additional terms for both matrices are $\mathbf{C}_1^{BW}[4,5] = \mathbf{C}_1^{BW}[7,8] = \mathbf{C}_2^{BW}[5,4] = \mathbf{C}_2^{BW}[8,7] = 2k_-(\kappa^S - \kappa^B)$.

For the second interface the situation is symmetric to the one presented above. For the last point of QW, e.g., z_k, the matrix $\mathbf{A}^{WB}(z_k)$ is equal $\mathbf{A}^{BW}(z_{j+1})$ and the matrix for the first point of the second barrier $\mathbf{A}^{WB}(z_{k+1})$ is equal to the matrix defined for the last point of the first QB namely $\mathbf{A}^{BW}(z_j)$. The matrices $\mathbf{B}^{WB}$ and $\mathbf{C}^{WB}$ are created in the same way.

Using this procedure the complex but Hermitian symmetric matrix can be obtained. Subsequently, the eigenenergy values and the corresponding eigenvectors are obtained from solving the eigenvalue of H_0 (and H' for $B \neq 0$).

4. Numerical Results

The results presented below were received for the band structure parameters collected in Table 1. All presented results are obtained for the case when both barriers are about 100 nm which in practice means infinite potential. To get a better agreement with the real structures of QW, three different regions were taken into account

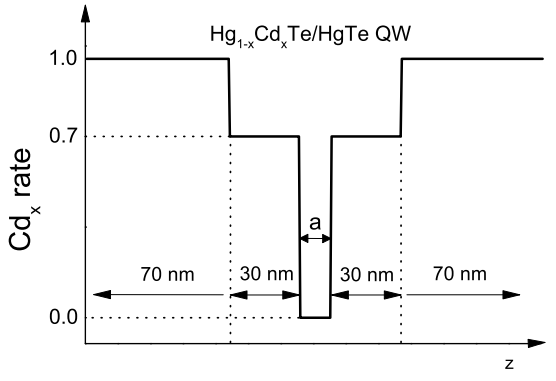

Fig. 2. The shape of potential of the investigated QW structures.

in the numerical calculation (see Fig. 2): the CdTe layer (70 nm) and the buffer layer $Hg_{0.3}Cd_{0.7}Te$ (30 nm) which are placed on both sides of the different widths of HgTe QW.

The distance between the nearest two points Δz is defined to be equal to half of the lattice constant of a unit cell. The dependencies of all parameters, except the bandgap, on the content of the solid solution $Hg_{1-x}Cd_xTe$ are assumed to be linear in x. To verify the validity of our proposed method and find the application range of this approach, the dispersion relations and the LLs' energy spectra for different widths of QW were calculated.

The dispersion relations for the potential profiles presented in Fig. 2 were calculated for two directions of k: $k_{||} = [11]$ and $k_{||} = [10]$ for $CdTe/Hg_{0.3}Cd_{0.7}Te/HgTe$ QW for different values of the width of QW and the results are presented in Fig. 3. It can be clearly seen that our results are in good agreement with the ones presented in the literature by other authors for the heterostructures with normal band structures[4,14] as well as with inverted band structures.[3,5,6,11,17]

The proposed method is then applied to calculate the LLs' energies for the investigated structures. In case of the magnetic field perpendicular to the layer ($B||z$), the FDM was used into the H' Hamiltonian. The structures of the electronic LLs are presented in Fig. 4. The number of LLs was marked in all figures which corresponds to normal [Figs. 4(a) and 4(b)] and inverted band structures [Figs. 4(c) and 4(d)].

For $a = 6$ nm the electron ($E1$) subband is still above the first heavy hole subband ($H2$)–similar like for 4 nm in Fig. 3(a) [the dispersion relation around Γ-point for 6 nm QW with energy gap of 4.5 meV is presented in the inset of Fig. 3(b)].

In case of inverted structures we get the energy dispersion [Figs. 3(c) and 3(d)] and LL spectra for $H1$, $H2$ and $E1$ subbands [Figs. 4(c) and 4(d)]. For $a = 12$ nm and $a = 14$ nm the electron subbands (E) are pushed below the levels occupied by heavy holes. In case of 12 nm QW the $E1$ subband is shifted below $H3$ subband [Fig. 3(c)] and for 14 nm QW below $H4$ subband [Fig. 3(d)].

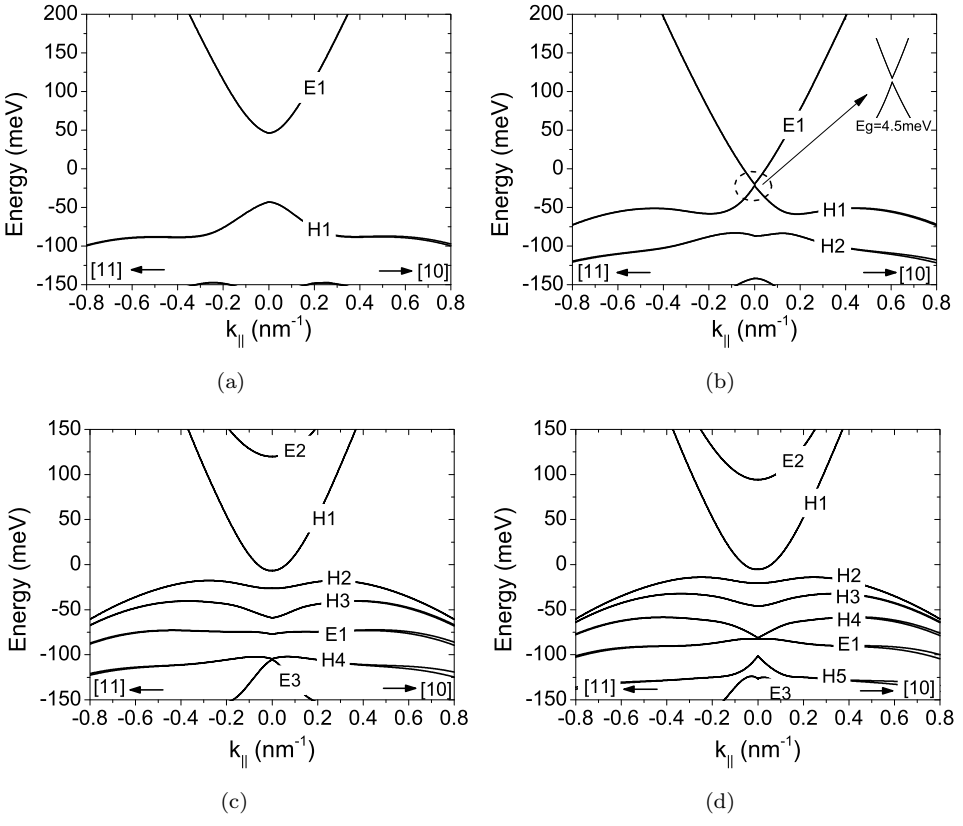

Fig. 3. Energy spectra of size-quantized subbands in a symmetric $CdTe/Hg_{0.3}Cd_{0.7}Te/HgTe$ QW for (a) $a = 4$ nm, (b) $a = 6$ nm, (c) $a = 12$ nm and (d) $a = 14$ nm QW widths calculated by FDM method applied for the 8×8 **kp** Kane Hamiltonian [Eq. (24)] for: $k_{||} = [10]$ and $k_{||} = [11]$.

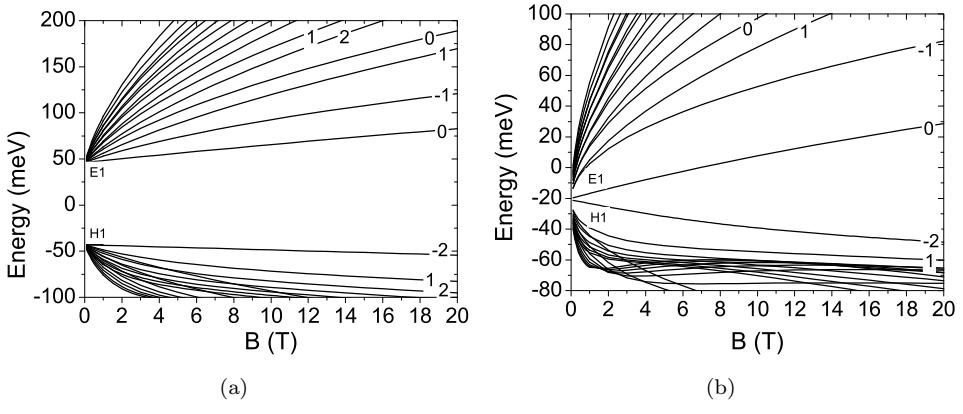

Fig. 4. Landau levels' energies for symmetric HgTe QW for: (a) $a = 4$ nm, (b) $a = 6$ nm, (c) $a = 12$ nm and (d) $a = 14$ nm QW widths calculated by FDM method applied for the 8×8 **kp** Kane Hamiltonian [Eq. (2.1)].

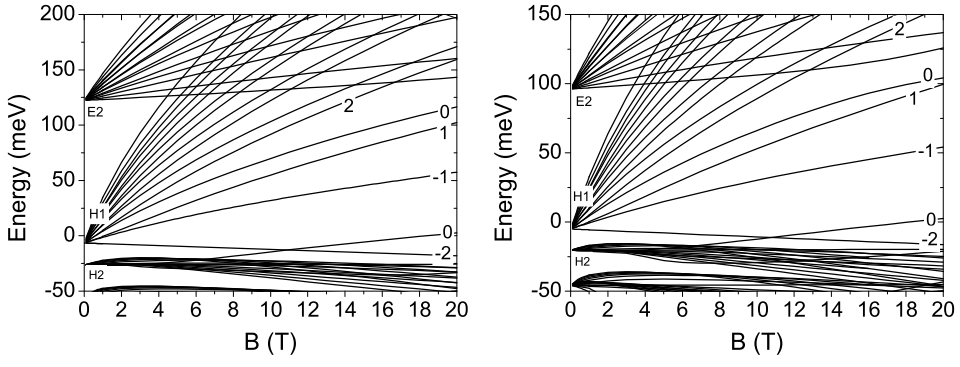

(c) (d)

Fig. 4. (*Continued*)

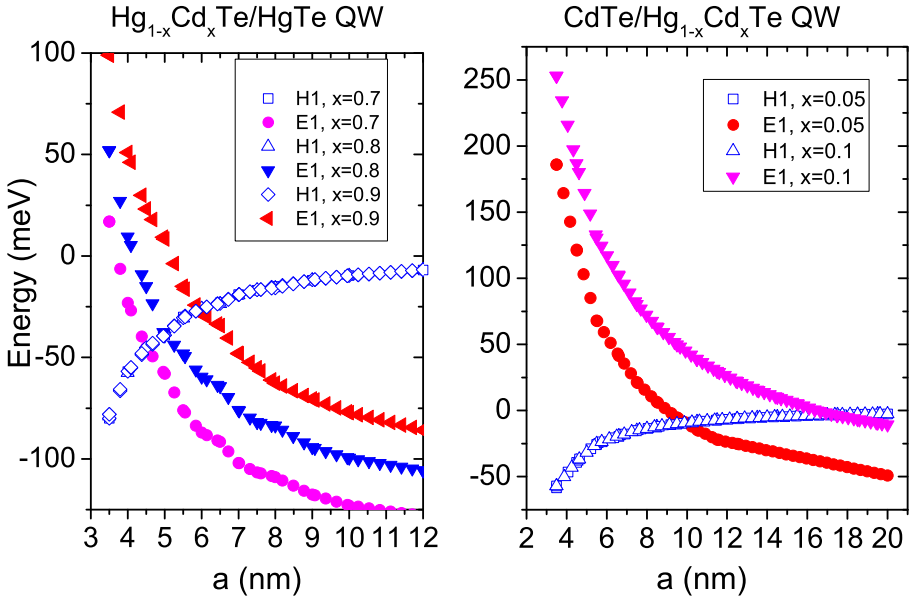

(a) (b)

Fig. 5. (Color online) Energies of the electron-like subband ($E1$) and hole-like subband ($H1$) as a function of the widths of QW: (a) with different x–Cd compounds in the barrier material in HgCdTe/HgTe QW and (b) with different x–Cd compounds in the QW material in CdTe/HgCdTe QW.

It is easy to see [Figs. 4(c) and 4(d)] that the lowest LL ($N = -2$) in the conduction band ($H1$) and the top LL ($N = 0$) in the valence band ($H2$) at about 11 T for 12 nm QW are crossed. These values are in good agreement with the values in previous works, see e.g., Ref. 36. However, the values (≈12 T) obtained by the authors of Ref. 36 where calculated for [211]-oriented QW.

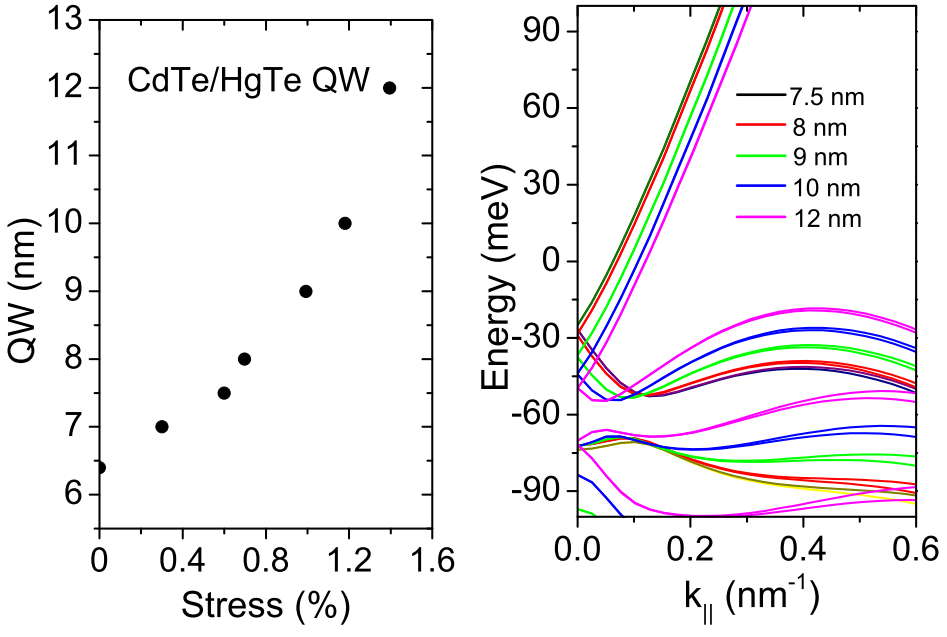

(a) (b)

Fig. 6. (Color online) (a) The QW widths as a function of the strain (lattice mismatch) for the structures with a Dirac point. (b) The $E(k_{||})$ for different HgTe QW widths were calculated for different mismatch levels of lattice constants so that each time a Dirac cone can be achieved for each QW. The parameters of the lattice mismatch for the following QWs are equal: 0.32% for 7.5 nm wide QW, 0.40% for 8 nm wide QW, 0.70% for 9 nm wide QW, 0.98% for 10 nm wide QW and 1.20% for 12 nm wide QW.

Using this method the critical width of QW for the mixed HgCdTe heterostructures were calculated for two cases when the different x–Cd compounds in the (i) QW and (ii) barriers are taken into consideration. The results are presented in Fig. 5.

In case when the barrier area is built by HgCdTe it is possible to obtain the Dirac point for QW which is thinner than a critical value of 6.4 nm for the pure HgTe [see Fig. 5(a)]. On the other hand, for the mixed material of QW the Dirac-like dispersion for the unstained structures can be received for the wider QW structures of about 10 nm for $Hg_{0.95}Cd_{0.05}Te$ QW and 17 nm for $Hg_{0.9}Cd_{0.1}Te$ QW see Fig. 5(b).

The question is if it is possible to obtain a strained QW with a Dirac point, then how does the dispersion relation looks like in such cases. The answer is presented in Fig. 6(b), where $E(k_{||})$ for different HgTe QW widths were calculated for different mismatch levels of lattice constants, so that each time a Dirac cone can be achieved for each QW. A wider QW needs a bigger lattice mismatch [see Fig. 6(a)], the bigger lattice mismatch caused the shape of the light hole subband to change. For

such structures with a small concentration it is possible to observe the influence of the lower part of the Dirac cone.

5. Conclusion

In this paper the scheme of FDM applied for the 8×8 **kp** Kane Hamiltonian is presented. The numerical calculation was made for the most popular heterostructures of type III based on $Hg_{1-x}Cd_xTe/HgTe$ QW.

The matrix scheme was developed for two Hamiltonians: H_0 for the case with no magnetic field and H' for the magnetic field perpendicular to the layer. The presented method allows to get the solution for the energy dispersion as well as for the LL spectrum for type-III heterostructures for a wide range of the widths of QW. The presented matrix for FDM is easy to be implemented because the discrete form is simple and the matrix elements of the component matrices are concise, which makes the presented method very convenient. This model could also be easily extended by adding the self-consistent potential for solving the differential Poisson[21] equation with the doping layers inside $Hg_{0.7}Cd_{0.3}Te$ materials which allows to get, e.g., asymmetric QW.

Using this method it was shown that in the case of mixed HgCdTe QW structures the critical width is different and is a function of the x–Cd compound in the barrier as well as in the QW material. As was shown the Dirac point can be obtained for 10 nm wide $Hg_{0.95}Cd_{0.05}Te$ QW and 17 nm wide $Hg_{0.9}Cd_{0.1}Te$ QW.

In the case of strained QW the results of the calculation are very promising. As shown by the other authors the theoretical and experimental investigations of both the upper and lower parts of the Dirac cones in case of HgTe QW provide lots of interesting results.[37–40] There are lots of other different possibilities to use the presented method, for example, in the case of different growth $[kkl]$-oriented QWs the corresponding terms[3,41] should be added along the $[kkl]$ growth directions. For the case of the so-called 3D topological insulator with strained HgTe layer (see, e.g., Ref. 42) and mixed 3D HgCdTe TI[43] the effect of strain due to lattice mismatch between HgTe and $Hg_{1-x}Cd_xTe$ should be taken into account by adding the Pikus–Bir deformation interaction matrix $D(\epsilon)$ defined by the deformation potential.[44] As it was shown in Ref. 43 the presented method allows to predict that the Dirac point can be localized inside the strained gap for the mixed 3D HgCdTe TI.

Acknowledgments

This work was supported by the Project WND-RPPK.01.03.00-18-053/12. of Podkarpacki Region Operational Programme, Poland.

Appendix A. Matrices for FDM

The complete 8×8 matrices for the **A** matrix take the forms

$\mathbf{A}_1(z)$

$$= \begin{bmatrix} (2F+1) & 0 & 0 & 0 & 0 & 0 & 0 & 0 \\ 0 & (2F+1) & 0 & 0 & 0 & 0 & 0 & 0 \\ 0 & 0 & -\gamma_1-\gamma_2 & 0 & 0 & 0 & 0 & 0 \\ 0 & 0 & 0 & -\gamma_1+\gamma_2 & 0 & 0 & -\sqrt{2}\gamma_2 & 0 \\ 0 & 0 & 0 & 0 & -\gamma_1+\gamma_2 & 0 & 0 & \sqrt{2}\gamma_2 \\ 0 & 0 & 0 & 0 & 0 & -\gamma_1-\gamma_2 & 0 & 0 \\ 0 & 0 & 0 & -\sqrt{2}\gamma_2 & 0 & 0 & -\gamma_1 & 0 \\ 0 & 0 & 0 & 0 & \sqrt{2}\gamma_2 & 0 & 0 & -\gamma_1 \end{bmatrix}, \tag{A.1}$$

$\mathbf{A}_2(z)$

$$= \begin{bmatrix} 0 & 0 & -\frac{1}{\sqrt{2}}Pk_+ & 0 & \frac{1}{\sqrt{6}}Pk_- & 0 & 0 & -\frac{1}{\sqrt{3}}Pk_- \\ 0 & 0 & 0 & -\frac{1}{\sqrt{6}}Pk_+ & 0 & \frac{1}{\sqrt{2}}Pk_- & -\frac{1}{\sqrt{3}}Pk_+ & 0 \\ -\frac{1}{\sqrt{2}}k_-P & 0 & 0 & 0 & R & 0 & 0 & -\sqrt{2}R \\ 0 & -\frac{1}{\sqrt{6}}k_-P & 0 & 0 & 0 & R & 0 & 0 \\ \frac{1}{\sqrt{6}}k_+P & 0 & R^\dagger & 0 & 0 & 0 & 0 & 0 \\ 0 & \frac{1}{\sqrt{2}}k_+P & 0 & R^\dagger & 0 & 0 & \sqrt{2}R^\dagger & 0 \\ 0 & -\frac{1}{\sqrt{3}}k_-P & 0 & 0 & 0 & \sqrt{2}R & 0 & 0 \\ -\frac{1}{\sqrt{3}}k_+P & 0 & -\sqrt{2}R^\dagger & 0 & 0 & 0 & 0 & 0 \end{bmatrix}, \tag{A.2}$$

$\mathbf{A}_3(z)$

$$= \begin{bmatrix} 2F+1 & 0 & 0 & 0 & 0 & 0 & 0 & 0 \\ 0 & 2F+1 & 0 & 0 & 0 & 0 & 0 & 0 \\ 0 & 0 & -\gamma_1+2\gamma_2 & 0 & 0 & 0 & 0 & 0 \\ 0 & 0 & 0 & -\gamma_1-2\gamma_2 & 0 & 0 & 2\sqrt{2}\gamma_2 & 0 \\ 0 & 0 & 0 & 0 & -\gamma_1-2\gamma_2 & 0 & 0 & -2\sqrt{2}\gamma_2 \\ 0 & 0 & 0 & 0 & 0 & -\gamma_1+2\gamma_2 & 0 & 0 \\ 0 & 0 & 0 & 2\sqrt{2}\gamma_2 & 0 & 0 & -\gamma_1 & 0 \\ 0 & 0 & 0 & 0 & -2\sqrt{2}\gamma_2 & 0 & 0 & -\gamma_1 \end{bmatrix}. \tag{A.3}$$

The $\mathbf{E}^q(z)$ matrix contains the values of $E_c(z)$, $E_v(z)$ and $\Delta(z)$ for the material of the quantum wells ($q = W$) or barriers ($q = B$):

$$\mathbf{E}^q(z) = \begin{bmatrix} E_c^q(z) & 0 & 0 & 0 & 0 & 0 & 0 & 0 \\ 0 & E_c^q(z) & 0 & 0 & 0 & 0 & 0 & 0 \\ 0 & 0 & E_c^q(z) + E_v^q(z) & 0 & 0 & 0 & 0 & 0 \\ 0 & 0 & 0 & E_c^q(z) - E_v^q(z) & 0 & 0 & 0 & 0 \\ 0 & 0 & 0 & 0 & E_c^q(z) - E_v^q(z)0 & 0 & 0 & \\ 0 & 0 & 0 & 0 & 0 & E_c^q(z) + E_v^q(z) & 0 & 0 \\ 0 & 0 & 0 & 0 & 0 & 0 & E_v^q(z) - \Delta^q & 0 \\ 0 & 0 & 0 & 0 & 0 & 0 & 0 & E_v^q(z) - \Delta^q \end{bmatrix}. \quad \text{(A.4)}$$

The elements of the $\mathbf{B}$ matrix are

$$\mathbf{B}_1(z) = \begin{bmatrix} 0 & 0 & 0 & \sqrt{\frac{2}{3}}P & 0 & 0 & -\frac{1}{\sqrt{3}}P & 0 \\ 0 & 0 & 0 & 0 & \sqrt{\frac{2}{3}}P & 0 & 0 & \frac{1}{\sqrt{3}}P \\ 0 & 0 & 0 & 2\sqrt{3}k_-\gamma_3 & 0 & 0 & -\sqrt{6}k_-\gamma_3 & 0 \\ \sqrt{\frac{2}{3}}P & 0 & 0 & 0 & 0 & 0 & 0 & \sqrt{6}\sqrt{3}k_-\gamma_3 \\ 0 & \sqrt{\frac{2}{3}}P & 0 & 0 & 0 & 0 & \sqrt{6}\sqrt{3}k_+\gamma_3 & 0 \\ 0 & 0 & 0 & 0 & -2\sqrt{3}k_+\gamma_3 & 0 & 0 & -\sqrt{6}k_+\gamma_3 \\ -\frac{1}{\sqrt{3}}P & 0 & 0 & 0 & 0 & 0 & 0 & 0 \\ 0 & \frac{1}{\sqrt{3}}P & 0 & 0 & 0 & 0 & 0 & 0 \end{bmatrix}, \tag{A.5}$$

$$\mathbf{B}_2(z) = \left(\frac{-i}{2\Delta z}\right)^{\dagger} \begin{bmatrix} 0 & 0 & 0 & 0 & 0 & 0 & 0 & 0 \\ 0 & 0 & 0 & 0 & 0 & 0 & 0 & 0 \\ 0 & 0 & 0 & 0 & 0 & 0 & 0 & 0 \\ 0 & 0 & -2\sqrt{3}k_-\gamma_3 & 0 & 0 & 0 & 0 & 0 \\ 0 & 0 & 0 & 0 & 0 & 2\sqrt{3}k_+\gamma_3 & 0 & 0 \\ 0 & 0 & 0 & 0 & 0 & 0 & 0 & 0 \\ 0 & 0 & -\sqrt{2}\sqrt{3}k_-\gamma_3 & 0 & -\sqrt{6}\sqrt{3}k_+\gamma_3 & 0 & 0 & 0 \\ 0 & 0 & 0 & -\sqrt{6}\sqrt{3}k_-\gamma_3 & 0 & \sqrt{2}\sqrt{3}k_+\gamma_3 & 0 & 0 \end{bmatrix}^{\dagger}. \tag{A.6}$$

The additional matrices which appear at the interface are given as follows:

$$\mathbf{B}_1^{BW} = \begin{bmatrix}
0 & 0 & 0 & \sqrt{\frac{2}{3}}P & 0 & 0 & -\frac{1}{\sqrt{3}}P & 0 \\
0 & 0 & 0 & 0 & \sqrt{\frac{2}{3}}P & 0 & 0 & \frac{1}{\sqrt{3}}P \\
0 & 0 & 0 & \begin{matrix}2\sqrt{3}k_-(\gamma_3^B+\gamma_3^S \\ +\kappa^B-\kappa^S)\end{matrix} & 0 & 0 & \begin{matrix}-\sqrt{6}k_-(\gamma_3^B+\gamma_3^S \\ +\kappa^B-\kappa^S)\end{matrix} & 0 \\
\sqrt{\frac{2}{3}}P & 0 & 0 & 0 & 2k_-(\kappa^B-\kappa^S) & 0 & 0 & \begin{matrix}\sqrt{6}\sqrt{3}k_-(\gamma_3^B+\gamma_3^S \\ -\frac{1}{3}(\kappa^B-\kappa^S))\end{matrix} \\
0 & \sqrt{\frac{2}{3}}P & 0 & 0 & 0 & 0 & \begin{matrix}\sqrt{6}\sqrt{3}k_+(\gamma_3^B+\gamma_3^S \\ -\frac{1}{3}(\kappa^B-\kappa^S))\end{matrix} & 0 \\
0 & 0 & 0 & 0 & \begin{matrix}-2\sqrt{3}k_+(\gamma_3^B+\gamma_3^S \\ +\kappa^B-\kappa^S)\end{matrix} & 0 & 0 & \begin{matrix}-\sqrt{6}k_+(\gamma_3^B+\gamma_3^S \\ +\kappa^B-\kappa^S)\end{matrix} \\
-\frac{1}{\sqrt{3}}P & 0 & 0 & 0 & 0 & 0 & 0 & 2k_-(\kappa^B-\kappa^S) \\
0 & \frac{1}{\sqrt{3}}P & 0 & 0 & 0 & 0 & 0 & 0
\end{bmatrix}, \quad \text{(A.7)}$$

$$\mathbf{B}_2^{BW} = \left[\begin{array}{cccccccc}
0 & 0 & 0 & 0 & 0 & 0 & 0 & 0 \\
0 & 0 & 0 & 0 & 0 & 0 & 0 & 0 \\
0 & 0 & 0 & 0 & 0 & 0 & 0 & 0 \\
0 & 0 & -2\sqrt{3}k_-(\gamma_3^B+\gamma_3^S) & 0 & 0 & 0 & 0 & 0 \\
 & & +\kappa^B-\kappa^S) & & & & & \\
0 & 0 & 0 & 2k_-(\kappa^B-\kappa^S) & 0 & 2\sqrt{3}k_+(\gamma_3^B+\gamma_3^S & 0 & 0 \\
 & & & & & +\kappa^B-\kappa^S) & & \\
0 & 0 & 0 & 0 & 0 & 0 & 0 & 0 \\
0 & 0 & -\sqrt{2}\sqrt{3}k_-(\gamma_3^B+\gamma_3^S & 0 & -\sqrt{6}\sqrt{3}k_+(\gamma_3^B+\gamma_3^S & 0 & 0 & 0 \\
 & & +\kappa^B-\kappa^S) & & -\frac{1}{3}(\kappa^B-\kappa^S)) & & & \\
0 & 0 & 0 & -\sqrt{6}\sqrt{3}k_-(\gamma_3^B+\gamma_3^S & 0 & \sqrt{2}\sqrt{3}k_+(\gamma_3^B+\gamma_3^S & 2k_-(\kappa^B-\kappa^S) & 0 \\
 & & & -\frac{1}{3}(\kappa^B-\kappa^S)) & & +\kappa^B-\kappa^S) & &
\end{array}\right]^{\dagger}. \tag{A.8}$$

References

1. N. F. Johnson *et al.*, *Phys. Rev. B* **41**, 3655 (1990).
2. A. Bernevig, T. Hughes and S. C. Zhang, *Science* **314**, 1757 (2006).
3. A. Pfeuffer-Jeschke, Ph.D. thesis, Bandstrucktur und Landau-Niveaus quecksilberhaltiger II-VI-Heterostrukturen Physikalisches Institut, Universitt Wűrzburg, Germany (2000).
4. A. Pfeuer-Jeschke *et al.*, *Physica B* **256–258**, 486 (1998).
5. G. Landwehr *et al.*, *Physica E* **6**, 713 (2000).
6. K. Ortner *et al.*, *Phys. Rev. B* **66**, 075322 (2002).
7. C. R. Becker *et al.*, *Thin Solid Films* **412**, 129 (2002).
8. Y. S. Gui *et al.*, *Europhys. Lett.* **65**, 393 (2003).
9. C. R. Becker *et al.*, *J. Supercond.* **16**, 625 (2003).
10. Y. S. Gui *et al.*, *Phys. Rev. B* **70**, 115328 (2004).
11. E. G. Novik *et al.*, *Phys. Rev. B* **72**, 035321 (2005).
12. M. Kőnig *et al.*, *J. Phys. Soc. Jpn.* **77**, 031007 (2008).
13. M. Orlita *et al.*, *Phys. Rev. B* **83**, 115307 (2011).
14. M. Zholudev *et al.*, *Phys. Rev. B* **86**, 205420 (2012).
15. M. S. Zholudev *et al.*, *Nanoscale Res. Lett.* **7**, 534 (2012).
16. E. O. Melezhik, J. V. Gumenjuk-Sichevska and S. A. Dvoretskii, *Semicond. Phys. Quantum Electron. Optoelectron.* **17**, 179 (2014).
17. G. M. Minkov *et al.*, *Phys. Rev. B* **88**, 155306 (2013).
18. L. R. Ram, K. H. Yoo and R. L. Aggarwal, *Phys. Rev. B* **38**, 6151 (1988).
19. K. H. Yoo, L. R. Ram-Mohan and D. F. Nelson, *Phys. Rev. B* **39**, 12808 (1989).
20. D. C. Hutchings, *Appl. Phys. Lett.* **55**, 1082 (1989).
21. P. Harrison, *Quantum Wells, Wires and Dots*, 2nd edn. (Wiley, New York, 2006).
22. K. Q. Le, *Microw. Opt. Technol. Lett.* **51**, 1 (2009).
23. W. Yang and K. Chang, *Phys. Rev. B* **72**, 233309 (2005).
24. W. Yang, K. Chang and S.-C. Zhang, *Phys. Rev. Lett.* **100**, 056602 (2008).
25. K. Chang and W.-K. Lou, *Phys. Rev. Lett.* **106**, 206802 (2011).
26. X. Ma *et al.*, *J. Appl. Phys.* **114**, 063101 (2013).
27. S.-F. Tsay *et al.*, *Phys. Rev. B* **56**, 13242 (1997).
28. J. D. Cooper *et al.*, *Appl. Phys. Lett.* **108**, 1131109 (2010).
29. Y. Jiang *et al.*, *J. Appl. Phys.* **116**, 173702 (2014).
30. C. R. Becker *et al.*, *Phys. Rev. B* **62**, 10353 (2000).
31. C. R. Pidgeon and R. N. Brown, *Phys. Rev.* **146**, 575 (1966).
32. M. H. Weiler, in *Defects, (HgCd)Se, (HgCd)Te*, eds. R. K. Willardson and A. C. Beer, Semiconductors and Semimetals, Vol. 16 (Academic Press, New York, 1981), p. 119.
33. C. Galeriu, Ph.D. thesis, **kp** theory of semiconductor nanostructures Worcester Polytechnic Institute, USA, 2005.
34. M. G. Burt, *J. Phys., Condens. Matter.* **11**, R53 (1999).
35. A. T. Meney, B. Gonul and E. P. OReilly, *Phys. Rev. B* **50**, 10893 (1994).
36. M. Schultz *et al.*, *Phys. Rev. B* **57**, 14772 (1998).
37. M. V. Durnev and S. A. Tarasenko, *Phys. Rev. B* **93**, 075434 (2016).
38. S. A. Tarasenko *et al.*, *Phys. Rev. B* **91**, 081302(R) (2015).
39. O. E. Raichev *et al.*, *Phys. Rev. B* **86**, 155320 (2012).
40. M. Pang and X. G. Wu, *Phys. Rev. B* **88**, 235309 (2013).
41. J. Los, A. Fasolino and A. Catellani, *Phys. Rev. B* **53**, 4630 (1996).
42. C. Brüne *et al.*, *Phys. Rev. Lett.* **106**, 126803 (2011).

43. M. Marchewka, *Physica E* **84**, 407 (2016).
44. G. L. Bir and G. E. Pikus, *Symmetry and Strain-Induced Effects in Semiconductors* (John Wiley and Sons, New York, 1974).